SARG: the high resolution spectrograph of TNG

R.G. Gratton [1] G. Bonanno[2] P. Bruno[2] A. Calí[2] R.U. Claudi[1] R. Cosentino[2], 3 S. Desidera[1] F. Diego[4] G.Farisato[1] G. Martorana[1] M. Rebeschini[1] S. Scuderi,[2]

[1] *Osservatorio Astronomico di Padova, Vicolo dell'Osservatorio, 5, I-35122 Padova, Italy*

[2] *Osservatorio Astrofisico, via S. Sofia, 78, I– 95123, Catania,Italy*

[3] *Centro Galileo Galilei, CNAA, Calle Alvarez de Abreu,70, 1st Floor 38700 Santa Cruz de La Palma, TF, Spain*

[4] *University College of London, Department of Physics and Astronomy, Gower Street, London WCLE 6BT,UK*

Abstract. SARG is a cross dispersed echelle spectrograph in operation since late spring 2000 at the Italian Telescopio Nazionale Galileo (TNG) 3.5 m telescope, La Palma. SARG offers both single object and long slit (up to 26 arcsec) observing modes covering a spectral range from $\lambda = 0.37$ up to 1 μm, with resolution ranging from R=29,000 up to R=164,000. Cross dispersion is provided by means of a selection of four grisms; interference filters may be used for the long slit mode (up to 26 arcsec). A dioptric camera images the cross dispersed spectra onto a mosaic of two 2048×4096 EEV CCDs (pixel size: 13.5 μm) allowing complete spectral coverage at all resolving power for $\lambda < 0.8$ μm. In order to reach a high wavelength calibration precision an iodine-absorbing cell is provided. A Distributed Active Temperature Control System (DATCS) mantains constant the temperature of all spectrograph components at a preset value. Early results show that SARG works according to original specifications in terms of wavelength coverage, efficiency (measured peak efficiency is about 13%), resolution (maximum resolution $R = 164,000$ using a 0.3 arcsec slit, $R \sim 144,000$ using an image slicer), and stability (preliminary estimates of radial velocity accuracy is ~ 3 m/s using the iodine cell and ± 150 m/s without the iodine cell).

Keywords: Instrumentation - Spectrographs

1. Introduction

SARG is the high resolution optical spectrograph for the Italian Galileo National Telescope (TNG). TNG is an alt-azimuth 3.5 m active telescope, located at 2400 m height on Roque de los Muchachos, La Palma, Canary Islands, Spain (Bortoletto et al. (1998)). TNG is presently the largest optical telescope offered to the italian astronomical community in the northern emisphere: it has been equipped with a quite complete set of instruments. SARG was designed as a multi-purpose instrument, in order to satisfy the scientific needs of a rather wide community, working on a variety of themes, ranging from stellar abundance analysis or extended objects, to line profile studies and accurate radial velocity

measurements. However, emphasis in the design was put to have a high resolution, stable instrument, while not sacrifying efficiency; such an instrument is particularly good for precise radial velocity programs, such as planet search and asteroseismology.

Instrument specifications included a high spectral resolution (maximum about $R \sim 150,000$), high efficiency (peak $> 10\%$ including telescope and detector), rather large spectral coverage in a single shot (two shots allowing to cover the entire accessible range from 370 to 900 nm; it was not possible to have high efficiency in the UV within budget limitations), high stability (long term stability of 5 m/s, and possibly 1 m/s over a single night). While meeting all these requirements required a complex and sophisticated instrument, design criteria also included simplicity of use and maintenance, and respect for the TNG standards and environment. The project (approved in February 1996) was scheduled as a four year project, and within a typical budget for a 4 m telescope class instrument. To realize such a complex instrument within the allowed budget, we had to take responsibility for the optical design and integration of the instrument. Approximately following the original schedule, SARG first spectra were obtained on the evening of June 9, 2000; SARG was offered to all the TNG community from January 2001, slightly less than five years after its approval. As we will show SARG performances are within the original specifications.

SARG was built as a collaboration of the astronomical observatories of Padova (optics, mechanics, thermal control, integration, science verification, project management), Catania (controls, software, detectors), Trieste and Palermo (management and science verification). The iodine cell was realized as the doctoral dissertation program of S. Desidera (Padova Observatory), with the collaboration of G. Favero (Dept. of Chemistry, Un. Padova) and A. Calí (Catania Observatory).

This paper presents a short description of some of the spectrograph properties and components, and of its performances.

2. Technical Characteristics

2.1. Overall features

The general layout of SARG is shown in Figures 1 and 2. SARG is permanently mounted on an optical table rigidly attached to the fork of TNG, about 1.4 m below the Nasmyth B focus (see Figure 1). Light reaches the spectrograph through an optical train which includes three lenses, and a folding mirror (FM1) which redirects light exiting horizontally along the elevation axis downward to the spectrograph

Figure 1. SARG layout in the TNG Nasmyth room B. On the foreground, the SARG electronic rack. Behind it, the SARG, rigidly mounted on the telescope fork. Light reaches the spectrograph from a folding mirror (in this picture hidden by the DoLoRes structure). The rotator adaptor is kept fixed when using SARG. Field derotation is achieved by means of an optical derotator. Guiding is done at the slit, using a cooled CCD.

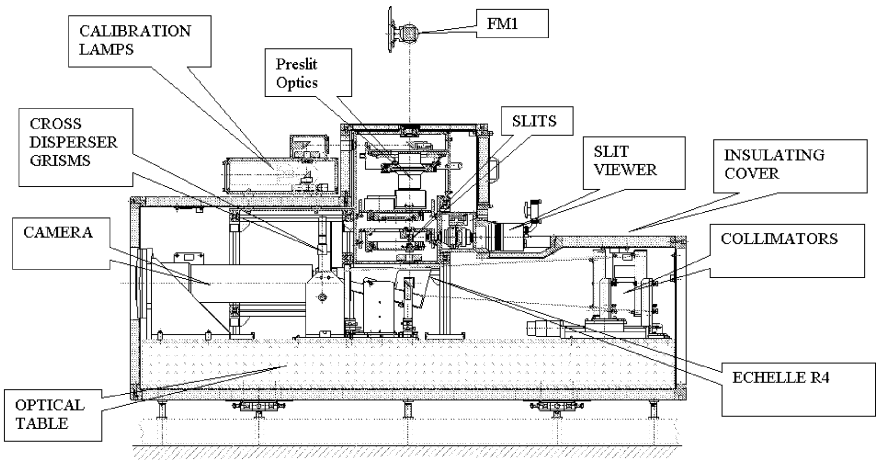

Figure 2. SARG layout. Light enters the spectrograph from top, after having being folded by a 45 degree mirror (FM1) shown rotated in this picture. Note (in order along the optical path) the calibration lamp unit, the preslit optics (including the optical derotator and the preslit slide equipped with the iodine cell), the slit wheel, the slit viewer, the spectrograph shutter, the white-pupil collimator, the R4 echelle, the wheel carrying the grisms used as cross dispersers, the dioptric camera, the optical table, and the insulating cover.

location. L1 and FM1 are mechanically located within DoLoRes (the TNG low dispersion spectrograph) which permanently occupies the Nasmyth B location (see Figure 1).

Note that due to SARG location, far from the Nasmyth focus, the TNG adapter rotator must be kept fixed while using SARG. Field derotation is provided by an optical derotator, and the standard TNG guiding camera of the derotator can not be used.

In analogy with several modern high resolution spectrographs, SARG has a white pupil collimator. This design, coupled with the use of an R4 echelle, of grism cross dispersing elements, and of a large field, quite long focal length dioptric camera exploiting a large size detector, composed of a mosaic of 2 $2k \times 4k$ CCDs, pixel size 13.5 μm, allowed a very compact and simple mechanical design. Instrument size is about $2 \times 1 \times 1$ m, small in view of the high spectral resolution achieved by the instrument when mounted on a 3.5 m telescope. This compact design also simplifies its thermal design: a special feature of SARG is its distributed active thermal control system (DATCS), which allows the spectrograph to have a nearly constant temperature of 19.5 ± 1.6 C while temperature in the Nasmyth B room changes from 0 to 20 C.

The preslit optics (which include a collimated part of the optical path) and the grism cross disperser also add flexibility to SARG, allow-

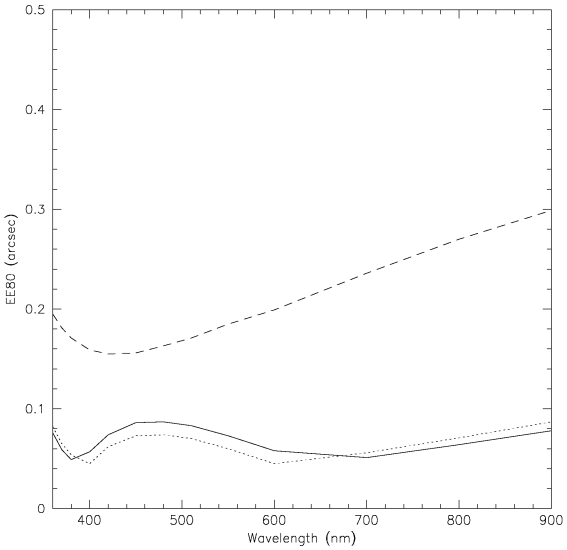

Figure 3. Geometrical optical quality of the preslit system (monochromatic 80% encircled energy) as a function of wavelength for three different position on the slit plane: field center (solid line), at 5 arcsec from field center (dotted line), and at 15 arcsec from field center, i.e. the edge of the unvignetted field (dashed line). The system is nearly diffraction limited at field center.

ing a variety of optical modes: multiorder short slit observations with a large spectral coverage; 26 arcsec single order long slit observations (an optical derotator allows to have an arbitrary fixed orientation of the slit projected on the sky); multiorder image slicer observations at very high spectral resolution, using a Diego modified Bowen - Walraven image slicer (Diego 1994); high precision radial velocity observations using an I_2 absorption cell (Marcy & Butler (1992)). Finally, a polarization analyzer was mounted in front of the spectrograph in March 2001.

3. Optics

3.1. Preslit Optics

The preslit optics (realized by Fisba Optiks) consists of three lenses: L1 is a Barlow lens (a cemented FPL53-K5 doublet) located 420 mm in front of the TNG nominal focus, which transforms the f/11 TNG beam into an f/34.4 one, allowing a suitable focal position far from the elevation axis (so that SARG would not interfere with DoLoRes). A second lens (L2: a fused silica- FPL53-fused silica triplet), located

after an intermediate focal position (used to insert the polarization analyzer), creates a collimated beam: owing to space limitations, the diameter of this beam had to be kept small (6 mm); a third f/11 lens (L3: FPL53-K5 doublet) focuses the beam onto the slit, where the scale is the same as at the TNG Nasmyth foci (187 μm/arcsec). The L2/L3 system is afocal, so that the spectrograph entrance pupil is effectively at infinite: this allows a cleaner optical design, with the echelle located exactly on a pupil image. The optical quality of the preslit system is given in Figure 3, where the monochromatic 80% encircled energy is given as a function of wavelength for three different position on the focal plane.

The preslit optics is very efficient, thanks to the use of multilayer AR-coatings (Supertrioline by Balzer). The efficiency curve of the preslit optics is given in Figure 4.

The collimated portion of the beam is used for a fused silica Abbe-König inverting prism (actually, cemented to L2 to reduce the number of optical surfaces), which allows accurate derotation over an unvignetted field of about 30 arcsec (projected on sky), as well as to position the slit on an arbitrary angle on the sky. Owing to the small size of the collimated beam in the preslit optics, alignment of the optical and mechanical axis of the derotator is very critical. This was realized directly at Fisba Optiks, working the derotator wheel (an annular rotating table constructed by CINEL, providing a very stable rotation axis, with no flipping). However, even after this paintaking procedure, there is a significant residual disalignment between the two axis, with a small tilting but a quite large decentering (about 400 μm). This results in a significant migration of the pupil while rotating the derotator. Alignment of the optical derotator within SARG was realized so that perfect centering of the pupil (negligible tilt and decentering) is achieved for a given position of the derotator (optimizing point source observations which does not require derotation, like precise radial velocities). Vignetting due to pupil migration causes loss of efficiency in other derotator positions: this can be seen e.g. as a variation of the spectrograph efficiency as a function of the derotator angle. This will be discussed again Section 8.3. However, the efficiency loss (peaking at about 20 %) was considered acceptable in view of the difficulties in achieving a perfect alignment of the optical derotator. Note that a software option has been implemented, allowing acquisition and guiding with the optical derotator fixed in the optimal position.

The preslit optics also include slides and wheels for neutral and coloured filters (allowing suppression of undesired light); the two calibrating systems of SARG (the lamp array, including three quartz iodine

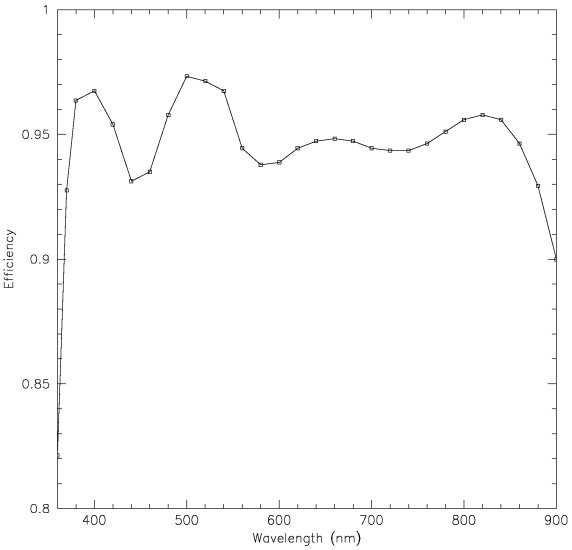

Figure 4. Optical efficiency of the preslit optics.

Table I. SARG slits

Ap.	Res.	Size (mm)	Size (arcsec)	Projected size (pixels)	Note
Hole					
#1	29,000	0.30×1.50	1.60×8.0	9.8×49.1	
#2	57,000	0.15×1.00	0.80×5.3	4.9×32.5	
#3	86,000	0.10×1.00	0.53×5.3	3.2×32.5	
#4	164,000	0.05×1.00	0.27×5.3	1.6×32.5	
#5	43,000	0.20×5.00	1.07×26.7	6.6×162.5	
#6	115,000	0.075×5.00	0.40×26.7	2.2×162.5	
#7	144,000	0.30×0.30	1.60×1.6	2.0×68.6	Image slicer
#8	115,000	0.075×1.70	0.40×9.0	2.2×40.8	Polarimetric mode

and a Th lamp; and the iodine absorption cell); and a slit viewer assembly.

3.2. Slits and Image slicer

The slit is actually a selection of 9 different apertures located on a motorized rotating table (also realized by CINEL), which allows resolution from $R = 29,000$ up to $R = 164,000$ (see Table I). Design

of the slit wheel emphasized stability of the aperture positions: the wheel is an annular table, with a large size ball-bearing that prevents flipping of the table. Movement of the wheel is controlled at very high precision (about 16 counts per μm along the slit length), and it is highly reproducible (r.m.s. of a few counts). Each slit has four axis micrometer movements. They were focused at a common focal position and aligned each other with an accuracy of $< 3\mu$m (peak-to-valley), corresponding to 0.015 arcsec projected on the sky, by a microscope providing a large magnification. This allows a great reproducibility in the position of the slits. The slits are mounted with an inclination of 10 degrees with respect to the optical beam, in order to feed the slit viewer. In order to optimize very high resolution observations in fair seeing conditions, one of the slit wheel positions is occupied by an image slicer realized by Francisco Diego (University College of London). This image slicer is of the Bowen-Walraven type, modified according to Diego (1994). It has an entrance square aperture (side 300 μm, that is 1.60 arcsec projected on the sky), located on the same focal position and with the same inclination of the other slits, so that centering of the object on it can be achieved using the same procedure used for the other apertures. The Diego version of the Bowen-Walraven image slicer has a small prism at the exit of the slicer, which compensate the optical path difference between the different slices, so that all the slices are at the same focal position; a second prism before the slicer compensates the dispersion given by the exit prism. To reduce the (very large) entrance angle to the image slicer, this was realized in a flint glass (SF-5); this choice minimizes reflection losses, so that total transmission of the image slicer is about 70 % (note that all air-glass surfaces were coated in MgF). The thickness of the slab where internal reflections occurs (generating the slices) was fixed at 85 μm, so that each slice corresponds to a slit of 60 μm (=0.32 arcsec on the sky), yielding an effective resolution of 144,000. Implementation of an image slicer within SARG was made difficult by the relatively short focal ratio used (f/11). The main consequence is that, since not all the slab can be on the focal plane, there are more than 5 slices (actually 10). In order to have a larger inter-order separation, three slices were sacrified by using an exit aperture, so that the image slicer generates 7 slices; the overall efficiency is then reduced to about 50 % (as measured on the quartz iodine comparison lamp spectrum). The projected slit length on the detector is 68.5 pixel=11.2 arcsec on the sky. Hence, adequate inter-order space for background subtraction is only available on the red halves of the spectra visualized with each grism. Bowen-Walraven image slicers cause an offset of the optical path; in our case this is about 5 mm. To avoid vignetting and a non-zero telecentric angle (that would greatly

reduce the efficiency of the image slicer), a binocular prism was inserted at the end of the image slicer: this prism recenters the optical path, so that the exit path is effectively aligned with the entrance one. In this way, the only optical effect of the image slicer is a small defocusing, that is compensated by moving the transfer collimator mirror (that is mounted on a motorized slide).

3.3. Slit Viewer

TNG pointing should be accurate to a few arcsec as required from the small SARG field of view, about 30 arcsec diameter. In this case the pointing of the telescope is made exploiting the slit viewer on board the spectrograph. Seldom the telescope accuracy has a fault and approximate centering of the star on the field may be done using the camera mounted on the TNG Rotator-Adapter, that can be inserted (and then removed) from the optical path. Following phases (acquisition and guiding) are done using the SARG Slit Viewer.

The SARG Slit Viewer is based on a double-stage (air) Peltier cooled scientific camera equipped with a frame transfer, front illuminated CCD EEV0520 (770×1152 pixels, 22.5μm pixel size). The slit viewer exploits a Nikon objective Nikkor 105 mm f/2.5 obtainig a scale of 0.137 arcsec/pixel. In front of the clear aperture of the objective, in the 10.9 mm collimated beam coming from the f=120 mm lens gathering the light reflected by the slit, it is possible to insert a 1.2 mm diaphragm and a blue filter by moving a commercial motorized slide. The diaphragm avoids to saturate the CCD when observing bright stars. The blue filter allows to properly center the star on the slit when using the blue grism.

The slit viewer allows then:

- to center the objects on the slit
- to focus the telescope
- to guide

The slit viewer camera is identical to the standard TNG camera used for guiding and Shack-Hartmann analysis on the TNG adapter rotators at the Nasmyth foci: centering and focusing of the objects on the slit are obtained with the same tools used by the other instruments. Due to the very small field of view (30 arcsec), the probability to find a guide-star with the slit viewer camera is very low. For this reason an algorithm based on the two spots rejected by the slit plate is used to guide during the exposition. At present, autoguiding is possible using a centroid based algorithm: this has shown to work quite well for slits not wider than about 1 arcsec. For larger slits, manual guiding is recommended.

Table II. SARG grisms and their main characteristics.

	BLUE	GREEN	YELLOW	RED
Spectral Range (nm)	369-518	419-567	462-795	502-1020
Peak efficency (%)	9.0	10.0	13.2	11.5
Min. separation (arcsec)	11.3	13.9	8.1	6.0

With the slit viewer camera, it is possible see objects as faint as magnitude 19 (in typical observing conditions, with a bright near full moon).

3.4. Collimator, Echelle and Cross Disperser

The spectrograph shutter is located after the slit; thereafter, a second folding mirror (FM2) redirects light toward the f/11 100 mm beam white-pupil collimator (constructed by SESO). This includes two off-axis parabolas (actually two segments of the same on-axis mirror), and a flat mirror (FM3) located close to the intermediate focus of the white pupil system (to fold the optical path saving space). The off-axis parabolas are properly oversized, to avoid vignetting for off-axis beams and to collect all useful light diffracted from the echelle grating. All collimator mirrors are silver coated, greatly enhancing efficiency in the visible and near IR, sacrifying UV.

In the first pupil image created by this system, we located the 31.6 gr/mm R4 echelle grating (useful area 400×96 mm) produced by Richardson Lab: this choice allows a quite high RS product of $RS = 46,000$. The echelle is used in a quasi-Littrow configuration (off-plane angle of 0.7 degrees). After alignment, the grating was locked in position by suitable screws. Also the echelle is coated in protected silver, to enhance efficiency in the visible. The whole free spectral range is visualized on the camera for wavelength shorter than 800 nm.

A selection of grisms (realized by FISBA Optik), mounted on a large size anular rotating table (realized by CINEL), are located in the second pupil image, allowing a variety of cross dispersion modes (see Table II).

To enhance efficiency, the flat surfaces of the grisms have a multilayer broad band AR coating appropriate for the wavelength range projected onto the detector; measured efficiency curves for each grism are shown in Figure 5. One further position on this table is left free, to be used for long slit observations coupled with interference filters located in the filter wheel in the preslit portion of the beam.

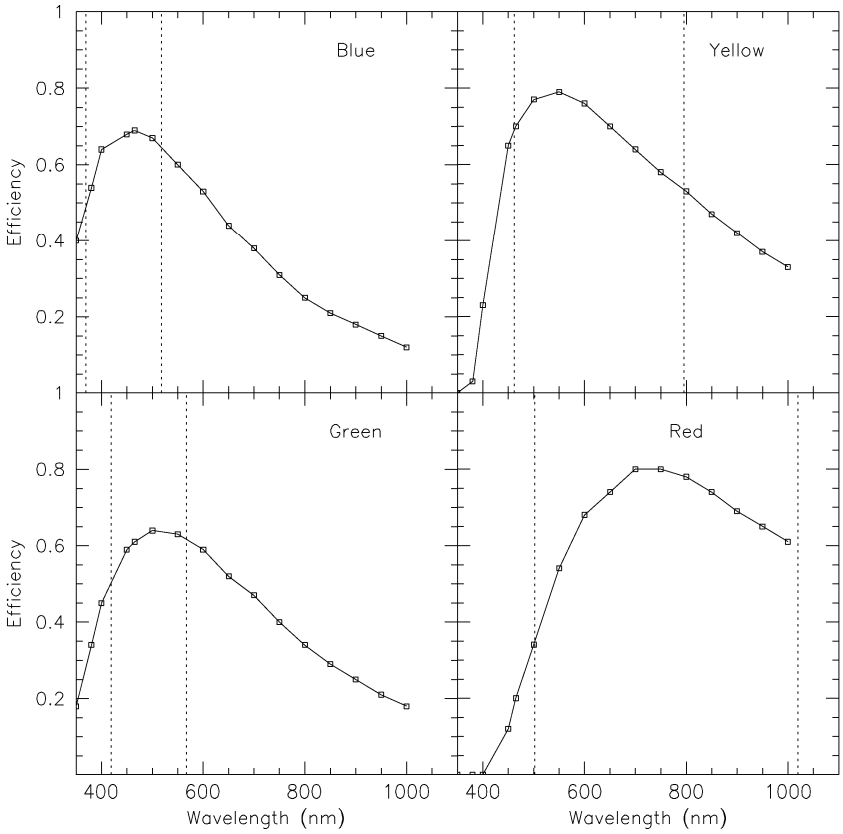

Figure 5. Efficiency of SARG grisms. For each grism the vertical dashed lines indicate the working wavelength range.

3.5. Camera and Detector

SARG uses a single, quite long (485 mm focal length, providing a scale of 0.16 arcsec/pixel when used at SARG), large field (8.5 degrees) dioptric camera constructed by SESO on our design. The camera (having a clear aperture of 116 mm) consists of five lenses, divided into three groups: a cemented triplet (FPL53-PSK3-FPL53), a thick FPL53 meniscus, and a fused silica field lens. All surfaces are spherical, but the last surface of the field lens that has a quite strong cylindrical power, in order to compensate for the field curvature introduced by the white pupil collimator. They have a broad-band AR coating (realized by SESO), enhancing efficiency. This camera has excellent performances. Optical quality is extremely good: the worst spot when the camera is used alone (see Figure 6) has a (monochromatic; lateral colour was not corrected

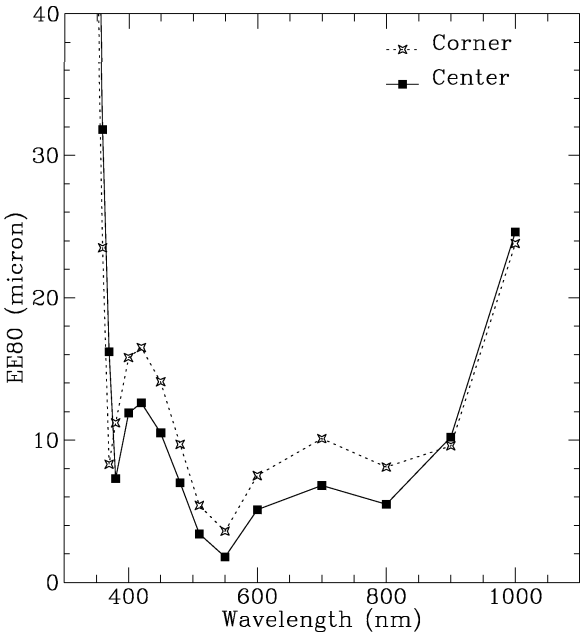

Figure 6. Optical quality (diameter of 80% Encircled Energy EE80) of SARG camera (used alone).

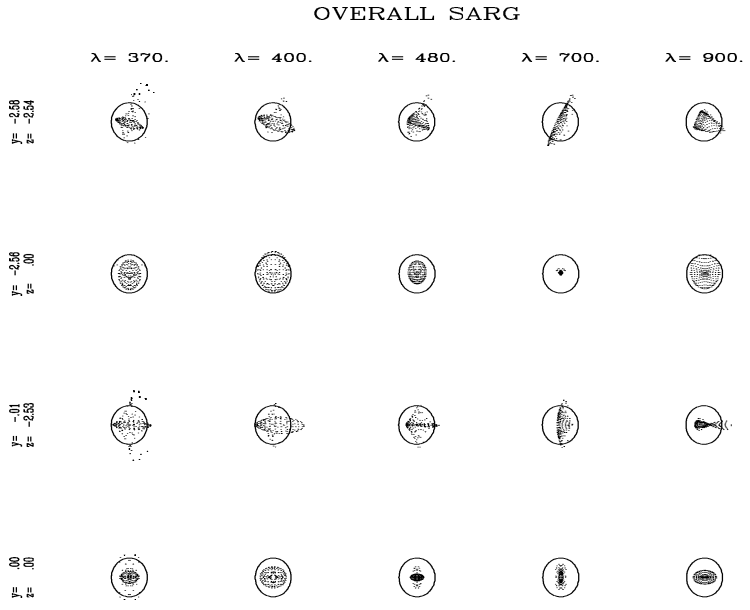

Figure 7. Spot diagram for SARG (from telescope to CCD focal plane).

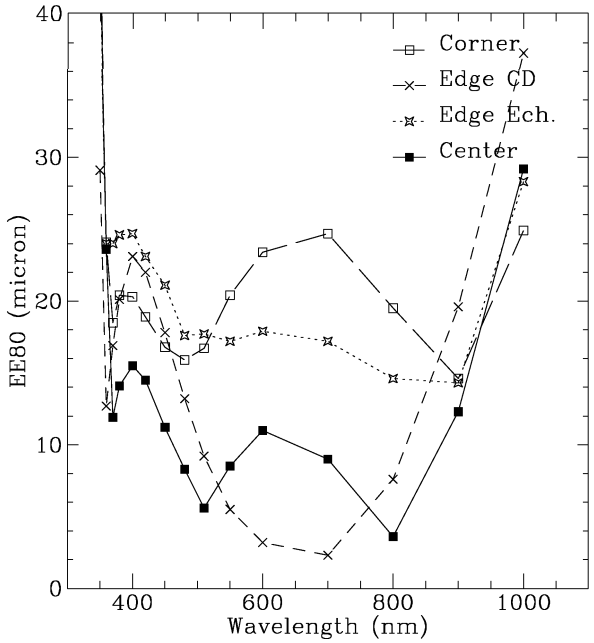

Figure 8. Optical quality (diameter of 80% Encircled Energy EE80) of SARG (from telescope to CCD focal plane).

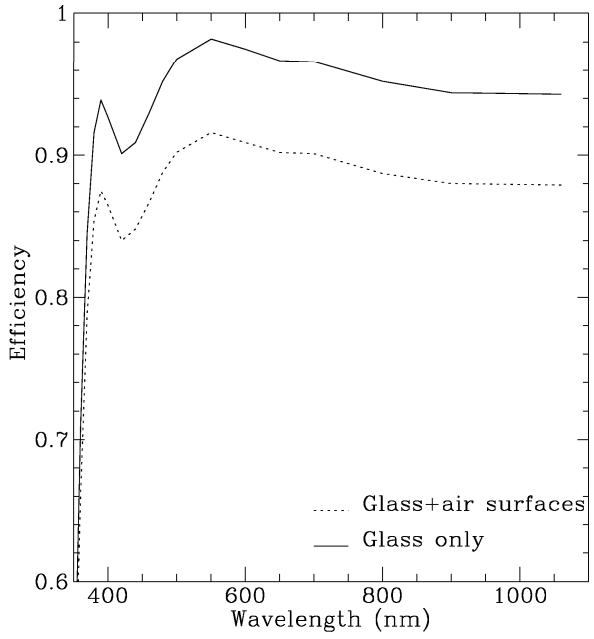

Figure 9. Efficiency of SARG camera.

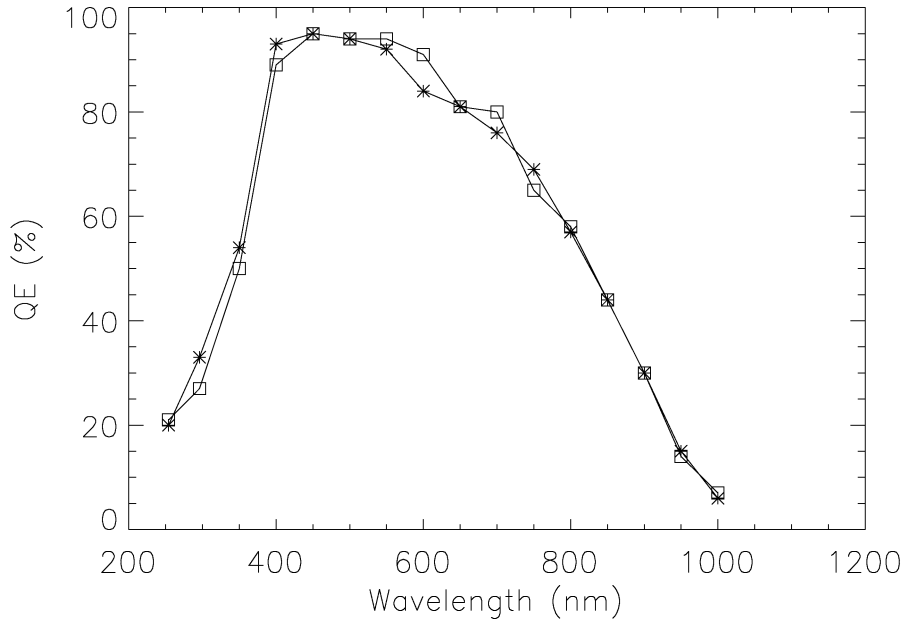

Figure 10. Efficiency of SARG CCD's. Blue side CCD: open squares; red side CCD: stars.

during optimization since this is a spectrograph camera) 80% encircled energy diameter of 18 μm over the whole spectral range 370-900 nm without refocusing over the whole field. Performances degradates a bit (to a worst spot with 80 % encircled energy of 24 μm: see Figures 7 and 8) when the whole telescope+spectrograph path is taken into account, however is still very good, yielding an expected maximum FWHM of the instrumental profile due to optics of 13 μm (=1 pixel) over the whole field. Indeed we see only limited degradation of the optical quality of the system even at the highest spectrograph resolution (164,000). Also the efficiency of the camera is very high (on average, 90 % over the useful spectral range 370-900 nm, with a minimum value of 84 % at the shortest useful wavelength of 370 nm: see Figure 9).

The detector is a mosaic of 2 thinned, back illuminated EEV $2k \times 4k$ CCDs, pixel 13.5 μm, providing a scale of 0.163 arcsec/pixel. CCD's long axis were positioned vertically, so that columns are aligned with echelle resolution: this minimizes the number of orders affected by the 400 μm (equivalent to about 30 pixels) gap between the two chips. Furthermore, the portion of the spectrum falling into this gap may be observed using a different grism. CCD chips are centered with the optical axis; however, since the sensitive area is not centered with the chips, this results in some decentering of the frames with respect to

the optical axis. Practically, order center (peak of the blaze function) occurs at a position 2400 along the CCD columns.

Measured efficiency of the CCD's as a function of wavelength is given in Figure 10. The CCD controller is a standard TNG system, realized by Elettromare. It allows to provide appropriate voltages to each CCD, and to read each of them from either single or double outputs using a 16 bits AD converter. The measured RON is 7.5 e^-, and the conversion factor is about 1.55 e^-/ADU, at a read-out rate of $\sim$ 60 Kpixels/sec. A variety of readout modes are implemented, allowing to bin the CCD (1×1, 1×2, 1×4, 2×1, 2×2, 2×4, 4×1, 4×2, 4×4). All these modes may be software selected through the SARG User Interface.

3.6. Anamorphosis and line – tilting

Effects of anamorphosis (due to the variation of the refraction angle at echelle along an order) and tilting of spectral lines (due to the off-plane angle) are large when using an R4.

Anamorphosis causes a variation of the scale (i.e. slit width projection and dispersion) along an order. The anamorphosis coefficient A is given by $A = \cos i / \cos d$, where i and d are the incidence and diffraction angles. The effect is large for SARG, since A changes from $A = 0.83$ to $A = 1.27$ at the extremes of the red orders giving a variation of the dispersion by a factor of 1.5. Line tilting is given by:

$$\frac{di}{d\gamma} = \sin\gamma \, \frac{\sin i + \sin d}{\cos\gamma \, \cos d},$$

where γ is the echelle off-plane angle. In our case, line inclination changes from 5.3 to 8.2 degrees at order extremes. However, given the off-axis angle (of 5.7 degrees) with which the collimator is illuminated by FM2, the slits are effectively rotated by a similar amount, so that the actual inclination of the lines changes from -0.4 to 2.4 degrees with respect to the CCD rows along an order. This should be considered when reducing spectra.

3.7. Calibration systems

Two calibration systems are available on SARG: (i) the Calibration Lamp Unit; and (ii) The Iodine Gas Cell.

The Calibration Lamp Unit may be used to feed the spectrograph with light provided by one lamp that may be software selected amongst a set of four by rotating a motorized stage carrying the Lamp Selection Mirror. Light from the lamp can be introduced into the optical path by means of a 45 degree folding flat located on the motorized Calibration Mirror Slide located in front of L2.

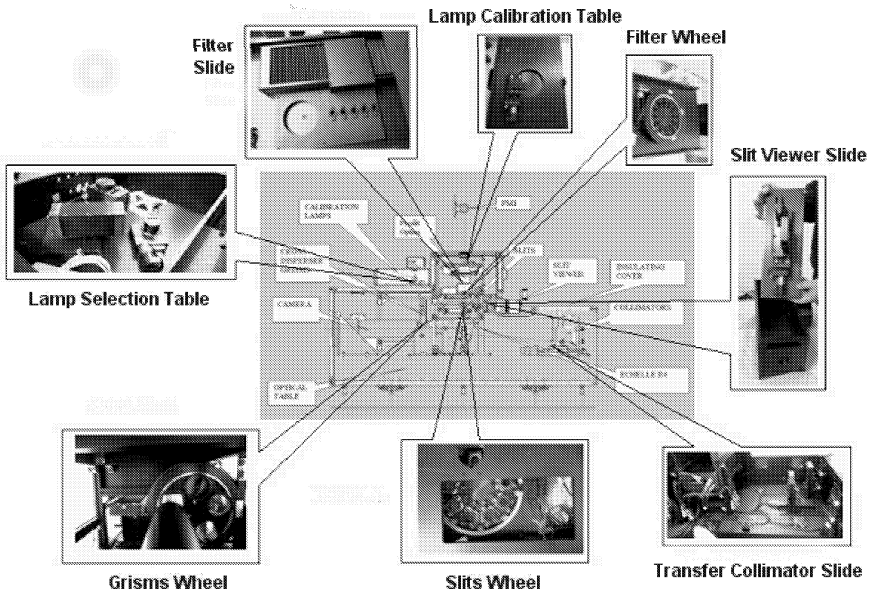

Figure 11. SARG motorized components.

The optics of the calibration lamp unit (realized using commercially available optics) was designed to efficiently and homogenously illuminate an area of at least 5.4 mm diameter in the slit plane (corresponding to 24 arcsec diameter) with a beam that is slightly faster than the telescope beam. Final definition of the entrance pupil of the instrument to F/11 is done by the pupil stop that is placed in the image of the telescope secondary (nominal size 6 mm). Some vignetting (due to L3) occurs at distances larger than 12 arcsec from field center.

The Calibration Lamp Array is a circular array of four lamps (three quartz iodine halogen lamp for flat fielding; a Th lamp for wavelength calibration). There are no specially devoted filters foreseen on the output of the diffusing element (although the neutral density filters mounted on the Preslit Slide can be used). However, in cross dispersed echelle spectroscopy, halogen flats can vary as much as a factor of 20-100 in intensity in a single frame due to the lower output of halogen in the UV, etc. For this reason, each halogen lamp is intended to be used with one particular cross disperser and have appropriate colour filters in front. This allows to balance the light output in order to reduce the dynamic range in flats.

An iodine gas cell (I_2 cell) may be inserted in the optical path to imprint on the object spectrum an absorption spectrum of I_2 lines which can be used as a very precise and stable wavelength reference.

The SARG I_2 cell is mounted on a specially devoted position on the Preslit Slide. The position of the I_2 cell allows also taking a lamp flat through the cell. This is useful for the calibration of the spectrograph, and for engineering tests of absolute stability and study of the instrumental profile.

4. Mechanics

SARG mechanics has been constructed by CINEL. It consists of three main components:

- The FM1 unit carries L1 and FM1. It is mounted on the input slide of DoLoRes
- The main spectrograph body includes the slit box (where the preslit optics is mounted), the calibration lamp unit, the slit viewer box, and the mountings for the main optical elements (collimator mirrors, echelle, grisms, camera). All these are located on a Newport optical table. The tables, and all the other elements (save for the calibration lamp and the CCD dewar) are located inside a thick thermally insulating enclosure. There are 9 motorized wheels and tables, that allow remote control of all spectrograph functions. Five of them are realized by means of commercial (OWIS) table; the remaining four are annular rotating tables realized by CINEL. Figure 11 illustrates the SARG motorized parts
- The Telescope/Spectrograph interface is a steel framework that allows proper handling and positioning of SARG at the arm of the TNG fork (fine alignment is achieved by tip/tilting a thick quartz window located within the optical path)

5. Controls

A sketch of overall architecture of SARG controls is given in Figure 12. It is a VME based system; the VME-bus directly controls the Elettromare TNG standard CCD controller by means of a fiber optics link and TNG standard Atenix boards. Instrument functions are controlled by RS232 links to stand-alone controllers (three OWIS motor-controller, a National Instruments board commanding the lamps, and a Lakeshore temperature monitor: see Figure 13). All these elements are located on a single rack, a couple of meters far from the spectrograph.

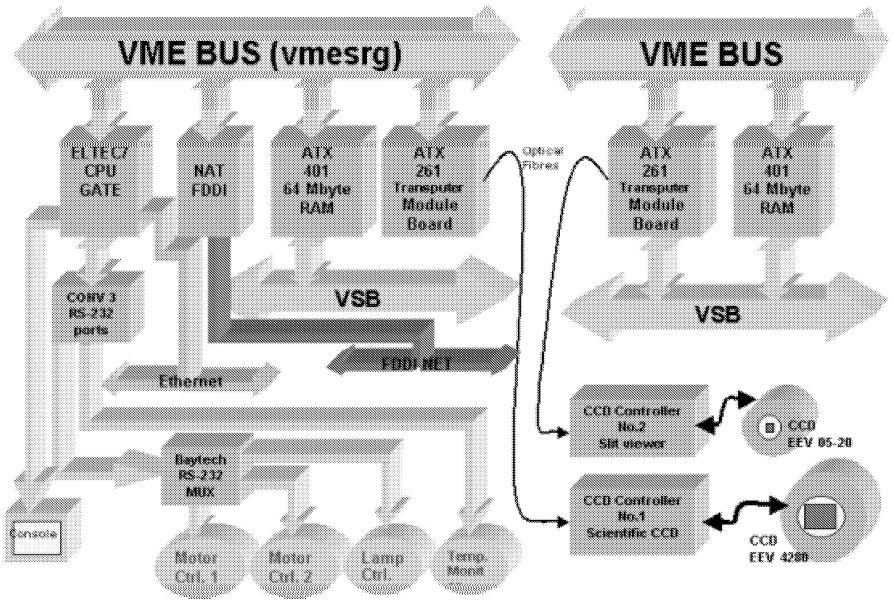

Figure 12. Architecture of SARG controls.

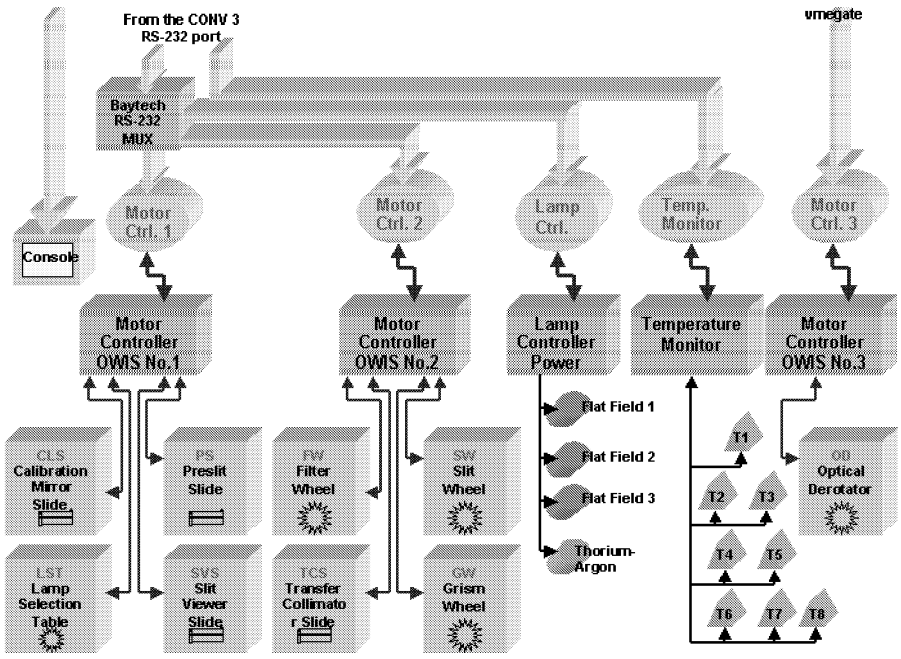

Figure 13. Scheme of low level SARG controls.

6. SARG Distributed Active Thermal Control System (DATCS)

Temperature within the SARG enclosure is kept approximately constant by means of an active thermal control system. The design of this system was done using a finite element computer model, tested against suitable laboratory experiments. The SARG thermal specifications were set as follows: (i) Long-term stability: < 0.5 C over 10 yr; (ii) Thermal inhomogeneities: < 1 C; (iii) Rate of temperature changes: < 1 C/hr. The spectrograph passive thermal properties are: (i) Weight: 750 kg; (ii) Effective Thermal capacity: 534 kJ/C; (iii) Heat Flux through enclosure: 10 W/C; (iv) Thermal Constant: 15 hr; (v) Total heat losses: 10-200 W (depending on environment temperature, expected to change seasonally from 0 to 19 C).

To achieve specifications, DATCS architecture consists of two main components:

- 30 MINCO CT 198 HEATERSTAT sensorless temperature controllers coupled with thermofoil resistances
- 8 DT-470 silicon diode sensors controlled by a Lakeshore 208 temperature Monitor

Within this design, particulare care was devoted to DATCS calibration. To this purposes, a special Heaterstat Calibration Box was constructed, a calibration procedure was defined and strictly enforced, and a maintenance plan was defined in order to mantain conditions stable over a long period of time.

From our computer model, we expected DATCS keep temperatures within SARG at 19.7 ± 0.7 C while the temperature in the Nasmyth room change from 0 to 19 C, the range given in TNG specifications (see Figure 14). The whole optomechanical design was based on this specifications: for instance, based on these values we do not expect that any refocusing of the spectrograph camera is required (actually the spectrograph might be refocused by moving the transfer collimator; however we foresee this possibility only when the image slicer is used). Strict procedures will be enforced to avoid that during spectrograph heating temperature gradients will not be larger than specifications.

7. Control software and User Interface

The full functionality of SARG is allowed by the software system of the spectrograph developed at C.O.L.D. (Catania Observatory Laboratory for Detectors). The low level software system (control software)

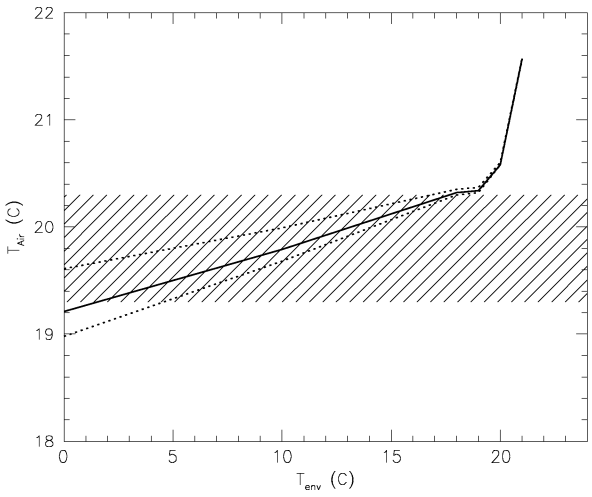

Figure 14. Run of the expected temperature inside the spectrograph as a function of ambient temperature: continuous line represents the average (air) temperature, while dotted lines are expected maximum and minimum values within the instrument. Dashed are represents the operational temperature (19.7 ± 0.7 C).

is deputed to control the different motorized movements, the lamps function and the CCDs controller. The high level software system (or User Interface) allows the observer to interact with the spectrograph and drive the observations.

7.1. Control Software

The SARG Control software is subdivided in two main frames: the maintenance control software and the service control software. The first is resident on a PC and is completely written in Visual Basic. It gives a clear Graphic User Interface (Fig. 15) in order to test and/or debug the individual motorized functions driving the movements of the spectrograph during stand alone operations. Using this work section it is possible to modify all the motor control parameters like PID filters or acceleration ramps and motor rotation velocities, simply editing tables. The new value of parameters or the motion commands are directed to the Motor control by a RS-232 connection. The service control software is the real control software. It is resident on the SARG VME, one of the PDOS machine of the Telescope VME network, under the GATE environment (Baruffolo and Bonoli (1992)) and it is completely written in ANSI C. The main functions are:

– it is deputed to translate the UIF command and direct then to the right subsystem

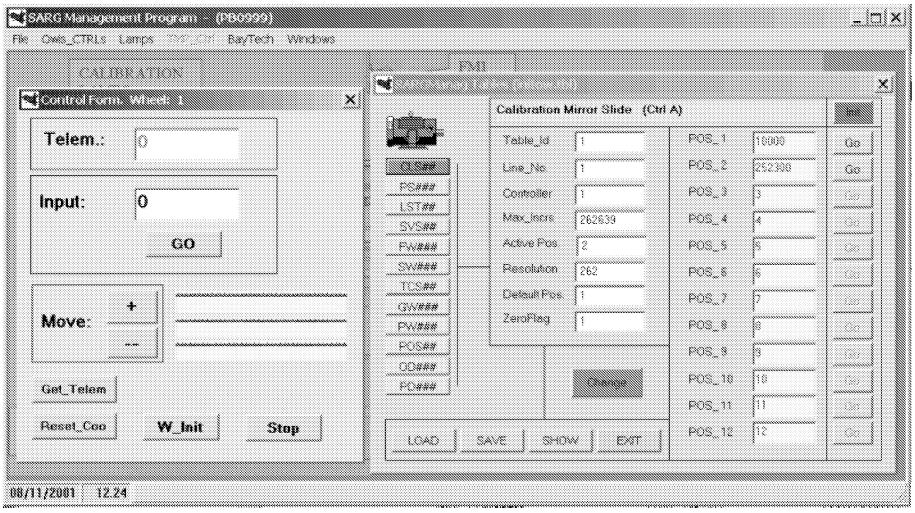

Figure 15. The main window of the graphic user interface of the standalone motor control software.

- it closes the position loop of the movement
- it transfers the telemetry on request
- it manages the error codes and it notifies them
- it provides for the network communication and synchronization with other telescope sub–systems
- it cyclically reads the temperature from probes housed in the spectrograph and in the instrument room
- it provides for a journal of the operations

7.2. User Interface

The SARG User Interface allows the observer to perform all operations necessary to manage the SARG spectrograph during an observational session. The User Interface is completely written using IDL software. It is composed of three different logical blocks which correspond to three different windows: an initialization window, a main window and a telemetry window.

The Initialization Window allows the observer to carry out all the operations necessary to initialize the CCD detectors and the mechanisms of the spectrograph. Limited on-line diagnostics is available in case of system faults, with suggestions for possible solutions of problems.

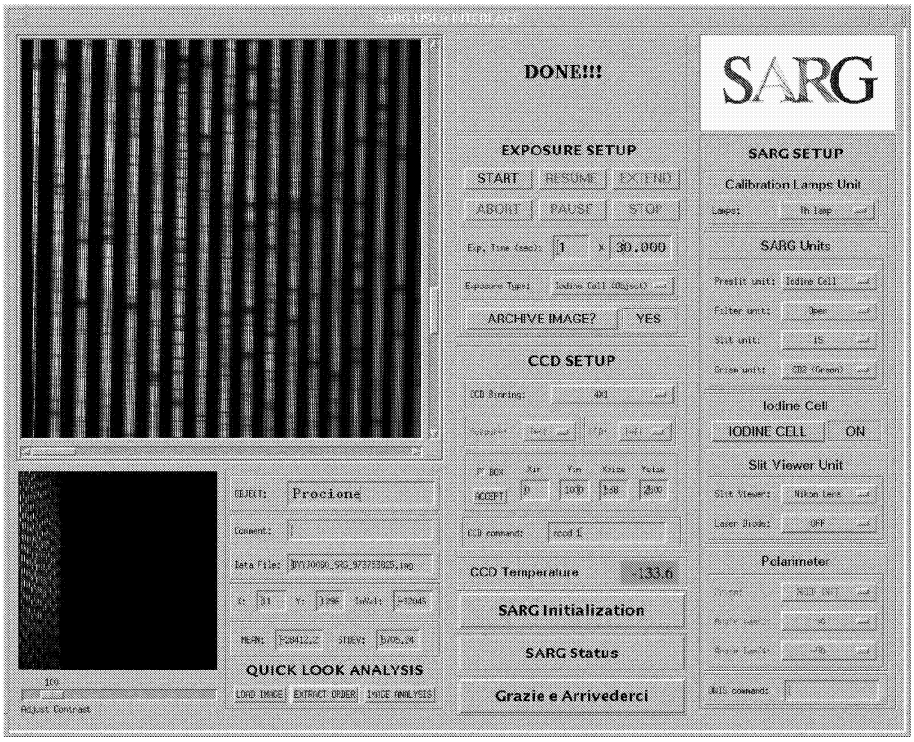

Figure 16. The main window of SARG user interface.

The time required to initialize a SARG mechanism goes from 15 seconds for the mechanism holding the Lamp Selection mirror to 195 seconds for the Grism Wheel, while the entire system is initialized in about 10 minutes. Note that full initialization is very rarely needed; positions given by the incremental encoders are stored on a permanent memory, so that they are usually recovered in case of system crashes.

The SARG main window is the core of the SARG user interface. It is not conceived as an "all in one window", in the sense that some operations (e.g. system initialization or telemtry) cannot be perfomed directly from it. As it can be seen from Figure 16 the SARG User Interface Main Window is composed of several different subwindows easy to identify.

The right part of the window contains the SARG SETUP subwindow which allows the observer to manage the whole spectrograph but the CCD detector. It is composed of 6 different working areas. The Calibration Lamp Unit area contains a pulldown menu to select one of the four available calibration lamps. In the SARG Unit area there are four different pulldown menus. They allow to move the preslit slide, holding a set of neutral filters and the iodine cell, the filter wheel,

holding a set of colored and interference filters, the slit wheel and the grism wheel. Selecting an element from a pulldown menu, the system moves the mechanism to the desired position. When selecting the image slicer (IS) from the Slit unit menu the Transfer Collimator Mirror is automatically moved to the position corresponding to the spectrograph focus with the image slicer and viceversa, that is, deselecting the image slicer makes the Transfer Collimator Mirror go back to the normal focus position. The Iodine Cell area contains a button to switch on and off the iodine cell and a window with the status of the cell. The Slit Viewer Unit area allows to move the slide which accomodates the blue filter or the diaphragm in front of the slit viewer camera. The Polarimeter area allow to manage the spectropolarimeter.

In the central column there is the EXPOSURE SETUP subwindow which allows to start/stop an exposure, to set the number of exposure, the exposure time and the exposure type and to archive an image. The CCD SETUP subwindow is used to set the CCD to be read, the binning, and the CCD outputs and to define a CCD subarea. Finally there are three utility buttons which allow to initialize SARG, to read the instrument's telemetry and to exit the interface.

The leftmost column has two graphic windows to show a full resolution and a rebinned image of the acquired spectrum. Furthermore there is a QUICK LOOK subwindow with three buttons which gives access to a number of reduction facilities, as order extraction, spatial and spectral resolution estimates, which allow the observer to assess on-line the quality of the data.

The SARG telemetry window allows the observer to know in real time the configuration of the spectrograph and of the detector. The user can retrieve information on the status of a single element or parameter, a group of them, or the complete configuration. It is divided in two main sections. The first section, devoted to the spectrograph, gives the status of all mechanisms and lamps inside SARG and also allows to monitor the temperature of the different part of the spectrograph. The second section is devoted to the CCD detectors and allows to obtain general information about the CCDs related temperatures, readout modes, biases and clocks.

8. SARG Performances

SARG has been in operation for more than one year with very little troubles, once the initially high background level was reduced to negligible values by appropriate tuning of the CCD voltages and screening of the encoder light leakages.

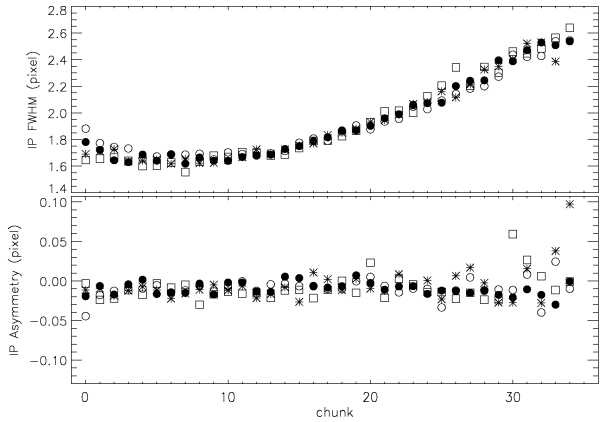

Figure 17. Run of the FWHM and of the asymmetry (defined as the difference between the left HWHM and the right HWHM) of instrumental profiles derived from a B star + Iodine for different spectral orders (120: empty circles; 115: filled circles; 111: asterisks; 106: open squares). Each chunk represents a portion of 101 pixels along dispersion.

In the following we describe some tests we have made to check proper working of the instrument.

8.1. Optical quality and resolution

Most critical tests of the SARG optical quality are those provided by the instrumental profiles (IPs) derived from study of the iodine lines. The software used to extract high precision radial velocities (AUSTRAL: Endl et al. (2000)) includes the reconstruction of the spectrograph instrument profile from the observed iodine cell spectrum, using as template the very high resolution ($R \sim 750,000$), high S/N (≥ 500) spectrum obtained with the Kitt Peak Fourier Transform Spectrograph (FTS). Rigorously, the output of AUSTRAL is not the instrument profile of the spectrograph, but rather it is the function that convolved with the FTS iodine spectrum better reproduces the observed spectrum. Thus the spectrograph instrument profile is given by the convolution of FTS instrument profile with the model function. However, in our case the FTS contribution is very small (FWHM of 0.0056 Å at 5300 Å, i.e. 0.30 pixels), less than the intrinsic broadening of iodine lines.

Figure 17 shows the run of the FWHM and of the asymmetry (defined as the difference between the left HWHM and the right HWHM) of instrumental profiles derived from a fast rotating B star + Iodine cell for different spectral orders, obtained with the narrowest slit (width: 50 μm, that is a projected slit width of 1.63 pixels at order center). The width of the instrumental profile shows a trend as a function of

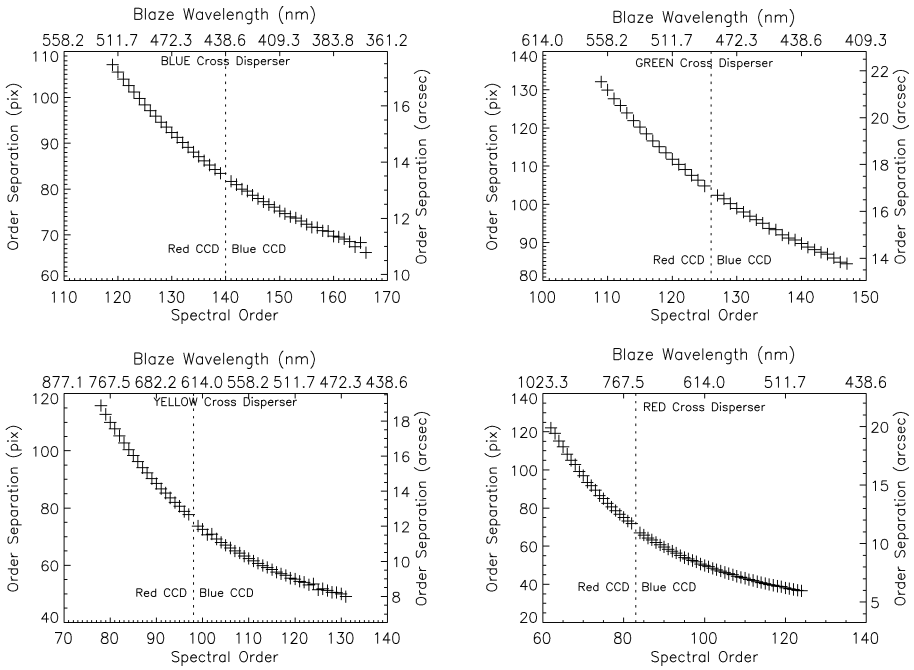

Figure 18. SARG Spectral format characteristics as measured with different grism cross dispersers.

the position along the order, changing on average by 40% level (from 1.6 to 2.4 pixels). Such a difference is due to the anamorphic magnification introduced by the R4 grating, that is changing from 0.83 to 1.27 at the extremes of the orders visualized on the CCD (that is, the projected slit width changes from 1.36 to 2.07 pixels: note that orders are not exactly centered on the CCD, the center being at chunk $\sim$ 10 on Figure 17). The slight curvature of the run of the FWHM (causing additional image broadening at blue and red edges of the order) is caused by a slight defocusing because the focal surface is not exactly planar. The instrumental profile shows a nearly symmetric shape. Differences between the left and right HWHM are below 3%.

From these tests we derive a typical FWHM at the order center of 1.68 pixels. Including the small contribution of Kitt Peak FTS to the intrinsic iodine spectrum, the resulting FWHM of SARG instrumental profile at the center of the order is 1.76 pixels. This corresponds to a resolving power of 164,000. Taking into account the projected slit width of 1.63 pixels, we derive that at order centers the optics contribution to the instrumental profile is 0.66 pixels, that is ~ 9 μm. As mentioned above, the optical quality is slightly worst at the extremes of an order,

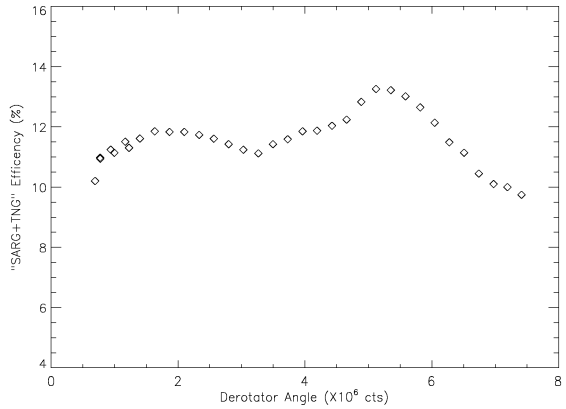

Figure 19. Efficiency of TNG+SARG as a function of the postion angle of the optical derotator.

where the contribution due to the optics may be as large as ~ 1.4 pixel (i.e. ~ 19 μm: slightly worst than the expected value of 13 μm).

Repeated experiments showed that these results were stable with time, indipendent of observing conditions (temperature etc). A further test of the overall optical quality of SARG + telescope system is provided by analysis of the FWHM of spectra in the direction perpendicular to dispersion. This of course includes not only broadening due to SARG optics, but also that due to the dome seeing at the epochs of observation. At present, best values of these FWHM are of 0.50 arcsec (these values were obtained with a binning of 2 along the direction perpendicular to dispersion, so that spectra were effectively severely undersampled in this direction).

8.2. Spectral formats

The optical characteristics described in the previous sections and the cross disperser choice allow a variety of observing modes. The number of the orders on the detectors together with the order separation and the order blaze wavelength for each cross disperser are given in Figure 18.

8.3. Efficiency

The misalignment between optical and mechanical axis of SARG derotator causes a pupil migration when changing derotator position; this causes some vignetting (on the filter unit, on the echelle and on the cross disperser). The efficiency of the spectrograph for different derotator positions was measured on September 13, 2000 by observing without a slit the star ζ Cas (see Figure 19). A maximum of efficiency (at 5200000

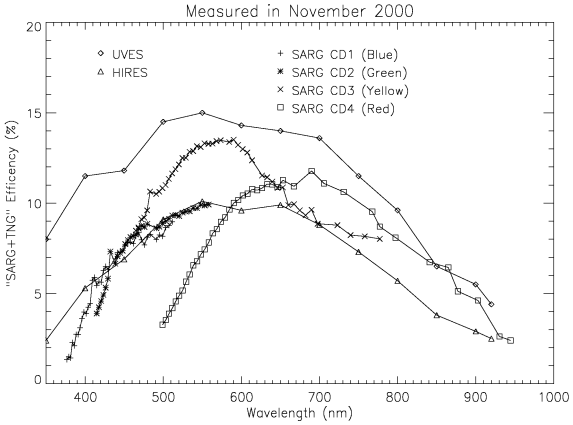

Figure 20. TNG+SARG efficiency (without slit) for all available grisms, measured observing the spectrophotometric standard 58 Aql on Nov. 5 2000. For comparison, similar measurements for UVES at Kueyen (VLT Unit 2) and HIRES at Keck are also shown.

counts) is clearly identified. Visual inspection of pupil footprints within the spectrograph showed that there is no vignetting when the derotator is in this position.

The efficiency of the spectrograph in various configurations (but with the derotator always in its optimal position) was measured on a photometric night (November 5, 2000) observing the spectrophotometric standard 58 Aql (HR 7596), again without any slit. The efficiency resulted higher than measured in September, because the TNG mirrors had been cleaned a few days before (note that TNG primary mirror was last aluminized in September 1999, about one year before the present tests). The measured efficiency of TNG+SARG using the four grisms is given in Figure 20. For comparison, similar results for UVES at Kueyen (VLT Unit 2), and HIRES at Keck are also given (they were obtained from the WEB). At peak wavelength, SARG+TNG efficiency is only slightly lower than that measured for Kueyen+UVES (however, TNG mirror coatings are likely somewhat less efficient than those of Kueyen), and well above the values obtained for Keck+HIRES.

8.4. Limiting magnitude

The spectrograph limiting magnitude was evaluated using the measured efficiency of TNG+SARG. We evaluate the limiting magnitude as the stellar magnitude (in the photometric band relative to the different grisms) that produce a SNR$\sim$ 10 in an exposure time of 1hr with the CCD binned 4×4 for the resolution R=29,000. The sky luminosity was

Table III. SARG limiting magnitudes (S/N=10 in 1 hr, see text)

Grism	Phot. Band	Wavelength (nm)	Limiting Magnitude
Blue	B	440	17.0
Green	B	440	17.2
Yellow	V	550	17.6
Red	R	640	17.0

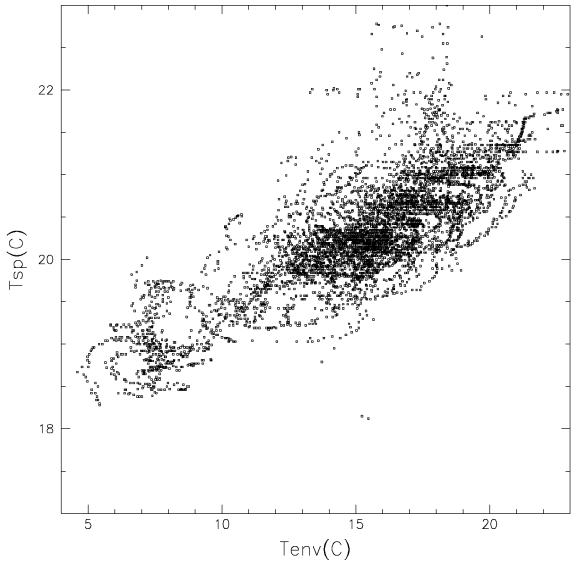

Figure 21. SARG temperature T_{sp} as a function of temperature in the TNG Nasmyth B room T_{env} during the period July-November 2000.

imposed to $m_{sky} = 21.4$ mag/arcsec^2 with a median seeing of 0.8 arcsec. The results are listed in Table III.

8.5. Thermal behavior and stability

As a test of the thermal behavior of SARG, we show in Figure 21 the run of the SARG temperature T_{sp} as a function of temperature in the TNG Nasmyth B room T_{env} during the period July-November 2000 (note that different sensors within the spectrograph yield the same results within 0.2 C). On the whole, temperature within the spectrograph changes by $\sim$ 0.16 C for a change of 1 degree in the temperature in

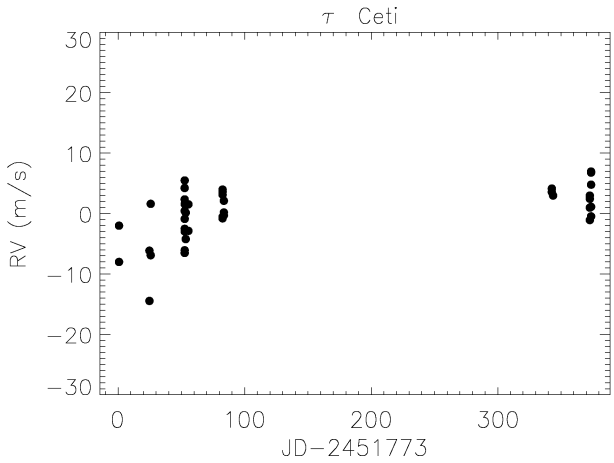

Figure 22. Preliminary radial velocities for the standard star τ Cet obtained from five orders. Full reduction will make use of the whole spectral region including lines of the iodine cell (about 25 orders).

the Nasmyth room. Since the expected temperature extremes in the Nasmyth room are 0 to 20 C, we expect a total temperature excursion of ± 1.6 C around a mean value of about 19.5 C. The sensitivity of SARG temperature to the external one is about twice the value expected on the basis of our models. This is due to larger than expected losses through the enclosure.We tried to reduce thermal losses from the spectrograph to the environment by protecting the spectrograph surface from the forced ventilation induced by the air conditioning system of the Nasmyth room (convection should dominate thermal exchanges from the spectrograph to the environment); however, no change in the sensitivity of the SARG temperature on environment was noticed.

The thickness of the relation between internal and external temperatures is due to the diurnal cycle and the delay in the reaction of internal temperatures to external changes. Typically, the amplitude of the diurnal oscillation in the Nasmyth room is about 3 C, with temperatures lower during the day (when the air conditioning system is working) than during the night (in this way the mirrors are slightly cooler than the expected night temperatures). The amplitude of diurnal temperature variations within the spectrograph are typically 0.5 C (peak–to–valley), with a delay of several hours with respect to the external temperature, so that each day a loop is described in Figure 21. Tests of optical quality have not revealed any degradation of image quality with changes in temperature, so that no refocusing was required.

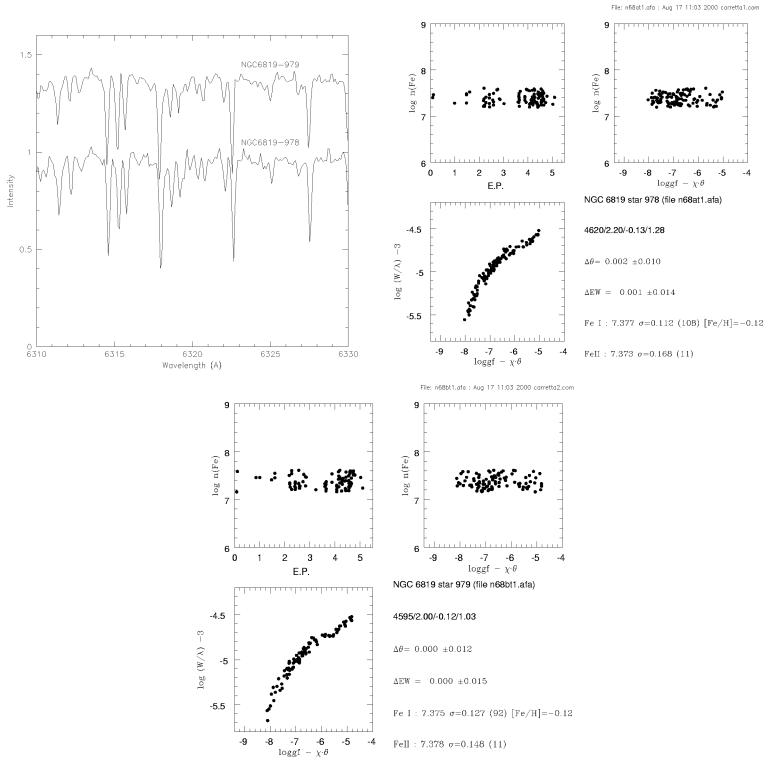

Figure 23. Representative graphs showing results obtained for the program on old open clusters. Note the extremely good definition of the curve obtained for stars with m>13.

8.6. Radial velocity precision

High precision radial velocities are one of the main targets of SARG. The whole potentiality of SARG in this field is still to be established. A first definition of the medium term (one month stability) of SARG radial velocities using the Iodine Cell is shown in Figure 22, which gives early results obtained from a preliminary analysis of 34 spectra of τ Cet, a star believed to have constant radial velocity. They were obtained using five orders, out of the about 25 covering the useful spectral regions with lines of the iodine cell. Note that spectra obtained during the two first runs were acquired in nights used to commission the instrument, so not in stable condition. The r.m.s. of these measurements is 3.3 m/s. We expect significant improvements from use of the full useful spectral range.

9. First Results

In this section we present a few early results obtained with SARG.

9.1. Abundances in old open clusters: NGC 6791 and NGC 6819 (Bragaglia et al. 2001)

We performed an analysis of high-dispersion spectra (R 40,000) of three red clump stars in the old open cluster NGC 6819. The spectra (see Figure 23) were analyzed using both equivalent widths measured with an automatic procedure and comparisons with synthetic spectra. NGC 6819 is found to be slightly metal-rich ([Fe/H]=+0.09 $\pm$ 0.03, internal error); there are no previous high-resolution studies to compare. Most element-to-element abundance ratios are close to solar; we find a slight excess of Si and a significant Na overabundance. Our spectra can also be used to derive the interstellar reddening toward the cluster by comparing the observed colors with those expected from line excitation: we derive E(B-V)=0.14$\pm$0.04, in agreement with the most recent estimate for this cluster.

9.2. P Cyg and AG Dra (Rossi et al. 2000)

This work concerns results of a preliminary analysis of the very high resolution spectrograms (R=86000) of P Cyg. A marked change in the H_α profile is noticed with respect of the May 1996 observations of Rossi et al. (Gäng (2000), see Figure 24). We also analyze the effect of the telluric lines on the spectral appearance by comparison with lower resolution observations, and find that it can simulate weak line variability.

9.3. St H_α (Munari et al. 2001)

A highly and rapidly variable bipolar mass outflow from StH_α 190 has been discovered, the first time in a yellow symbiotic star. Permitted emission lines are flanked by symmetrical jet features and multi-component P Cyg profiles, with velocities up to 300 km s^{-1}. Given the high orbital inclination of the binary, if the jets leave the system nearly perpendicular to the orbital plane, the de-projected velocity equals or exceeds the escape velocity (1000 km s^{-1}). StH_α 190 looks quite peculiar in many other respects: the hot component is an O-type subdwarf without an accretion disk or a veiling nebular continuum and the cool component is a G7 III star rotating at a spectacular 105 km s^{-1}, unseen by a large margin in field G giants (see Figure 25).

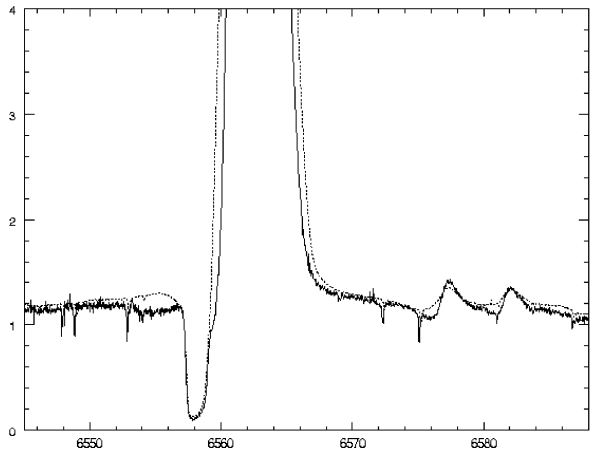

Figure 24. H_α profile variation at very high resolution. The June 2000 SARG spectrum (solid line) is compared with that of May 1996 (from Rossi et al. 2000).

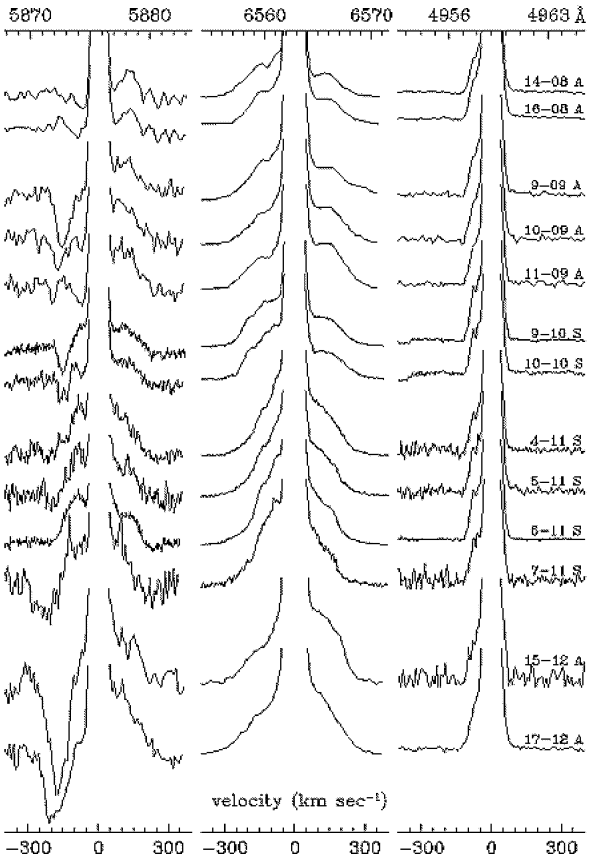

Figure 25. Evolution of the He I emission line profiles over a 4 month period (see dates on the right); SARG spectra are indicated with an S after the date.

9.4. Tomography of selected planetary nebulae (Sabbadin, Ragazzoni, reduction in progress)

In the preliminary results obtained from the thomography of NGC6572, obtained at SARG (red grism; 5 min. exposure; spectral resolution 115,000) it is possible to highlight (see Figure 26 (*Upper Panel*)) representative emission line structures at P.A.=0^o. In this reproduction the observed intensities are enhanced (by the factor indicated in parenthesis) to make each line comparable with H_α. Note the blurred appearance in H_α (mainly due to thermal motions) and the large stratification effects present in the nebula: low ionization emission, such as [OI] and [NII], occur in the external, faster layers, whereas the high excitation ones, [ArIII] and [OIII], are located in the internal, slower expanding regions. In Figure 26 (*Middle Panel*) main [OIII] λ5007 Å, H_α and [NII] λ6584 Å position – velocity structures observed at four position angles of NGC6572 (instrument configuration as before) are shown. The intensities of [OIII] and [NII] have been scaled to H_α. In Figure 26 (*Bottom Panel*) it is possible to see the same that before, but at higher contrast, to show the faintest [OIII] H_α and [NII] structures present in the 5 min spectra.

9.5. Non interacting main sequence binaries with different chemical compositions: Evidences of infall of rocky material? (Gratton et al. 2001)

We performed a careful differential abundance analysis of individual components of six main sequence binaries with separations of a few hundreds of AU. To reduce analysis concerns, we selected systems with almost equal mass components. We were able to derive differential abundances of several elements with errors down to 0.01 dex in the best cases. We found that in four systems the two components have the same chemical composition, within these very severe limits. However, clear differences were found for the two remaining systems (HD 219542 and HD 200466), in both cases the primaries being more Fe-rich than the secondaries, by 0.091 ± 0.009 and 0.053 ± 0.024 dex respectively (see Figure 27). Similar differences were found for most of the elements considered in our analysis; however, we found no appreciable difference for volatile elements and a trend for increasing abundance differences with increasing condensation temperature for individual elements, a result similar to that found for some single stars with planets by Smith et al. ((2001)). Finally, we note that HD 219542A has a Li-abundance comparable to those of Li-rich stars in old open clusters, while no Li is detected in the slightly cooler HD 219542B. We suggest that the primaries of these two systems have accreted rocky planets or the

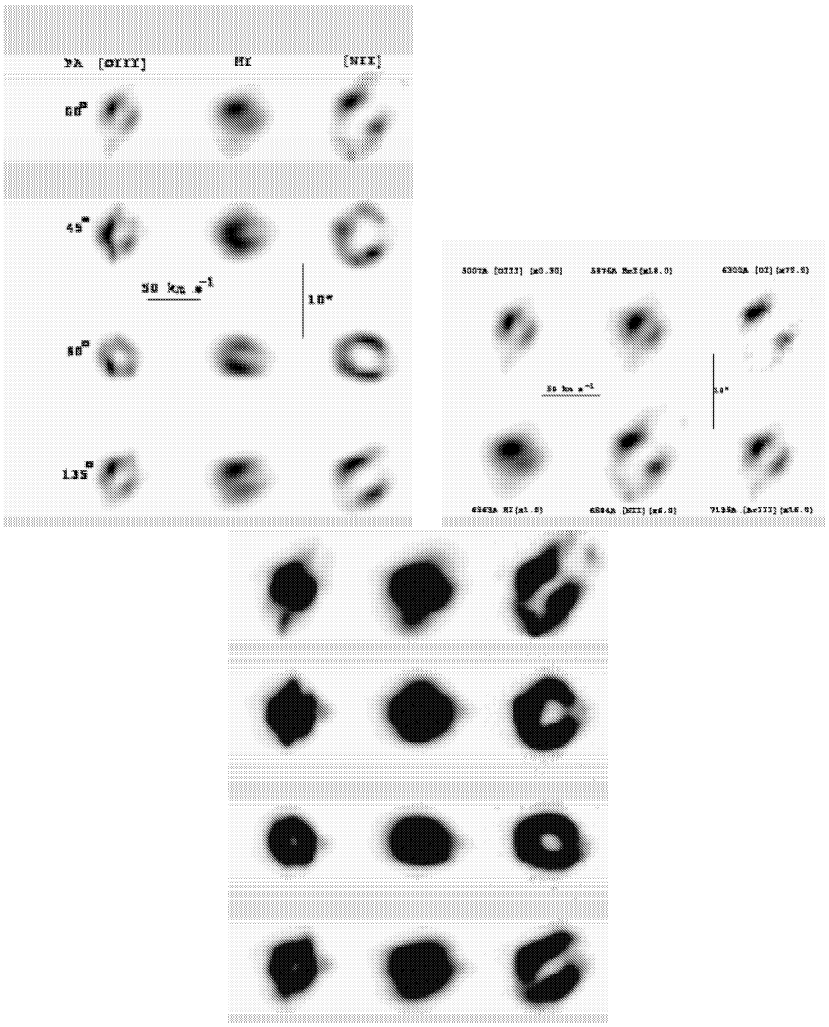

Figure 26. see the text

inner dust-rich part of a protoplanetary disk, likely due to gravitational perturbation caused by the presence of the companion.

Acknowledgements

The authors have a long list of people to thank: R. Bathia, A. Cavazza and F. Ferretti for the assistance in design phase of the instrument. P. Conconi for help in the mechanical design of the SARG camera. L. Contri, G. Giannesini, D. Strazzabosco and I. Rigoni of the Astronomical Observatory of Padova for the fundamental mechanical works. M.C.

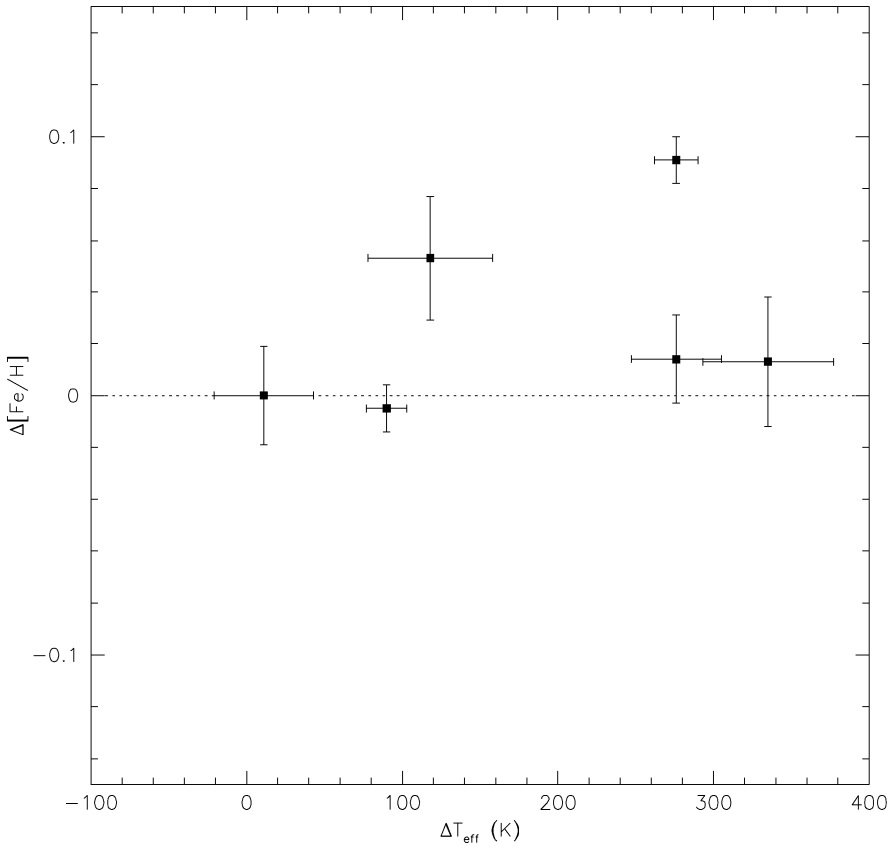

Figure 27. Run of the differences between the abundances obtained for the two components of each system with the difference in the effective temperatures adopted for the stars.

Timpanaro for cabling some part of the spectrograph. G. Favero for assistance at his chemical laboratory in building the iodine absorption cell. The directors of the Astronomical Observatory of Padova: G.F. De Zotti and M. Calvani for their suggestions and the innumerable signatures on contracts and documents; the administrative staff of the Astronomical Observatory (in particular Mrs. M. Locatelli and Mrs. D.Faro) to stand us with asiatic resignation. R. Pallavicini and P. Molaro for having contributed to the project with their C.N.R. funds. The director of CNAA M. Rodonò for his encouragement. S. D'Odorico and H. Dekker for technical assistance and for having provided designs of UVES, used as a template in the design of our instrument. M. Küster and M. Endl for the cooperation and their permission to use AUSTRAL for SARG. M. D'Alessandro and F. Bortoletto for assistance during laboratory work phases of the project. Dulick M. for the assistance in

obtaining the I_2 FTS spectrum at Keat Peak Observatory. A special thanks is due to G. Marino (CGG staff) and to the TNG Staff for the support given in this project.

References

Baruffolo A., Bonoli C.: GATE environment and module description, 1992, Padova Astron. Obs.

Bortoletto, F., Bonoli, C., D'Alessandro, M., Ragazzoni, R., Conconi, P., Mancini, D., Pucillo, M. 1998, in Astronomical telescopes and Instrumentation, SPIE, 3352, 91

Bragaglia, A.; Carretta, E.; Gratton, R. G.; Tosi, M.; Bonanno, G.; Bruno, P.; Calì, A.; Claudi, R.; Cosentino, R.; Desidera, S.; Farisato, G.; Rebeschini, M.; Scuderi, S., 2001, AJ, 121, 327

Diego, F. 1994, in Instrumentation in Astronomy VIII, eds. D.L. Crawford & E.R. Craine, SPIE, 2198, 525

Endl M., Küster M., Els S., 2000, A&A, 362, 585

Gäng, Th. 2000, Ph. D. Thesis, University of Heidelberg (http://chippawa.nascom.nasa.gov/gaang/)

Gratton R. G.; Bonanno G.; Claudi R.U.; Cosentino R.; Desidera S.; Lucatello S.; Scuderi S.; 2001, A&A, 377,123

Marcy G.W., Butler R.P., 1992, PASP, 104, 270

Munari, U.; Tomov, T.; Yudin, B. F.; Marrese, P. M.; Zwitter, T.; Gratton, R. G.; Bonanno, G.; Bruno, P.; Calì, A.; Claudi, R. U.; Cosentino, R.; Desidera, S.; Farisato, G.; Martorana, G.; Marino, G.; Rebeschini, M.; Scuderi, S.; Timpanaro, M. C.; 2001,A&A, 369, L1

Rossi C.; Viotti R.; Gang T.; Gratton, R. G.; Tosi, M.; Bonanno, G.; Bruno, P.; Calì, A.; Claudi, R.; Cosentino, R.; Desidera, S.; Farisato, G.; Rebeschini, M.; Scuderi, S., 2000,in "P Cygni 2000, 400 years of progress", Armagh, 21–23, August 2000 in Press

Smith V.V., Cunha K., Lazzaro D., 2001, AJ, 121,3207